

A Comprehensive Study on Microwave Imaging System for Breast Cancer Detection and Confocal Microwave Imaging

SAMIRAN KUMAR MANDAL¹

Instructor (Electronics Technology)

Shariatpur Polytechnic Institute, Bangladesh

SAZAL KUMAR SAMADDER

Instructor (Computer)

Ministry of Women & Children Affairs, DBWCTP (64 District)

Jatiyo Mohila Sangstha, Shariatpur, Bangladesh

Abstract

Breast cancer is one of the most commonly diagnosed cancers in females. Early breast cancer detection which has recently been gaining a lot of consideration within the research community and the most important for a quick and effective treatment of the cancer is early detection. Confocal microwave imaging algorithm is best for early breast cancer detection and is also one of the most promising and attractive screening techniques currently under research. This technique offers several advantages such as low cost, better patient comfort, non-ionizing and non-invasive radiation compared to X-Ray mammography. In this technique the breast is illuminated from various points with short UWB microwave pulse(s) and the collected backscattered energy is then processed to identify the presence and location of the tumor. In this thesis experimental measurement of the reflection coefficient in complex frequency domain is obtained from Vector Network Analyzer when the antenna is exposed to the environment and when the antenna is exposed to breast phantom. The tumor is simulated with different materials to investigate the effectiveness of the Confocal Microwave Imaging Algorithm for breast cancer detection. In addition, we used the materials at different depths to determine the effect of antenna distance to that of the tumor

¹ Both authors contributed equally in this work

response. The Confocal Microwave Imaging (CMI) Algorithm for breast cancer detection is an easy and robust technique for tumor detection, which is used to approximate the precise location of the tumor. CMI is based on illuminating the breast with the UWB pulse from different antenna locations. The relative arrival times & amplitudes of the backscatter signals is used to estimate the location of the tumor. We applied the Confocal Algorithm in this study to the numerical data generated with the VNA and analyzed the results with different material(s) as tumor at different depth to verify its ability to estimate a tumor response.

Keywords: Microwave Imaging System, Breast Cancer Detection, Confocal Microwave Imaging

INTRODUCTION:

Confocal Microwave Imaging (CMI) is slowly progressing from the theoretical stage involving extensive simulations to experimental feasibility studies. Two aspects need to be addressed: (i) the practical capability of CMI to detect tissue abnormalities, and (ii) verification of the hypothesis that large contrast exists between electrical parameters of breast cancer and normal breast tissue. In this paper we present initial results on both aspects of the technology. Creating images based on the dielectric properties of biological tissues at microwave frequencies is of increasing interest due to the potential for new and valuable medical diagnostic information. The nonionizing and potentially low cost aspects of microwave imaging are also appealing. Microwave imaging systems developed for clinical application incorporate radar-based techniques [1], [2], tomographic imaging [3], [4], or analysis of data collected at a number of sensors [5]. Tomographic images provide estimates of the dielectric properties of the imaging region, while radar-based techniques provide a scattering map related to changes in dielectric properties.

Microwave imaging has been of interest for many years for tumor detection. The advantage of microwave imaging includes wide range of frequencies, capability to focus the energy, ranges of simulation tools, less health risk and less

expensive. Presently, microwave imaging for early tumor detection has successfully gained attention due to the current advancements in imaging algorithms. Microwave imaging is a non-ionizing technique which is without doubt inexpensive compared to MRI and X-ray, and therefore is considered as an alternative imaging technique for breast cancer detection in the future [5].

Breast cancer has become one of the most widespread diseases worldwide making it a threat to the women of our society [2-5]. The technological boom in every aspect has made researchers to ponder over a screening tool that can be used to detect tumor in its developing stage, which can be used by the surgeons for further diagnosis [10]. Researchers have been trying to develop a way to utilize non-ionizing electromagnetic waves to image the human body in order to detect cancer. Recently, significant progress has been made towards breast cancer detection [3]. In the advent of ten years it is likely that microwave systems will become a possible solution. Breast tumors have electrical properties at microwave frequencies, which are different in contrast to healthy or normal breast tissue [11]. X-Ray being a known technology to detect breast cancer has reportedly caused side-effects to the breast tissues of the patient under examination. Researchers have implemented ultra-wide band radar based microwave imaging techniques, and have found it to be a potential modality for early detection of breast tumor in the recent years to come and the advantages can be noted as follows [3]: Low cost implementation; Exposure to non-harmful radiation; High accuracy; Better patient comfort compared to the currently used X-Ray mammography.

For detection of small tumor(s), a consistent contrast between tumor and normal breast tissues is required. Medical imaging methods have been applied to breast cancer detection with various degrees of success [12]. Ultrasound is used to determine whether the detected lesion is a liquid cyst or a solid tumor. Magnetic resonance imaging, is useful to examine embedded tumors, but expensive as a screening tool [12]. Methods to detect cancerous tissues are based on different physical properties being, tissue elasticity, temperature, and optical or electrical characteristics. We are particularly interested in techniques that employ electrical

property contrasts. Active approaches for breast tumor detection are currently being researched in the microwave frequency range.

Ultra-wideband (UWB) Radar imaging of the breast uses the difference in dielectric strengths of normal and cancerous tissue, in microwave frequency ranges [7]. Imaging techniques are then applied on the backscattered signal to construct an estimated image of the examined breast tissue [13]. Figure 1.1 shows the basic principle of tumor detection in a breast where a signal is transmitted through an antenna and the received signal is then processed to determine the location and size of tumor.

A number of imaging algorithms have been presented by many researchers. In this report experimental results obtained to evaluate the effectiveness of Confocal Microwave Imaging Algorithm with different materials as tumor. A number of imaging algorithms have been presented by many researchers. In this report experimental results of UWB microwave imaging system for radar-based breast cancer detection were obtained to evaluate the effectiveness of Confocal Microwave Imaging Algorithm with different materials as tumor.

The dissemination of breast cancer disease is reported to increase rapidly due to the shortcomings in the currently used screening methods, where X-ray mammography is the widely used screening technique amongst MRI and Ultrasound to detect breast tumors; however it has been reported to have estimated false results for around 30% of women who have had a screening [7-8]. The considerable amount of false results obtained is noticeably the limitation of the present screening methods in analyzing dense breast tissue and the area where the tumor might be located close to the chest or under the arm and mainly the estimation of early stage tumors [14]. Nowadays, researchers are employing microwave imaging techniques for non-invasive testing of breast cancer. The presence of tumor is being detected by comparing the dielectric properties of cancerous and normal breast tissues for detecting breast cancer.

The motivation of using the microwave techniques to diagnose a patient with breast cancer at the early stage is beneficial. In this thesis we demonstrate the experimental setup to review the confocal imaging algorithm which is used in radar based breast cancer

detection with high concern in reducing the amount of clutter in the backscatter signal(s) to investigate its effectiveness for different materials as tumor. In addition, we use the materials at different depths to identify the effect of antenna distance to that of the tumor response.

METHODS:

Instrumentation. This section discusses the experimental setup in detail which was used to analyze the effectiveness of confocal microwave imaging algorithm for different materials as tumor. The current technique for radar based microwave imaging consist of transmitting short pulse into the breast phantom and processing the collected reflections. Due to the difficulty on hardware for producing ultra-wideband pulses and fulfill the requirements for high dynamic range and measurement accuracy, all the experimental set up for pulse based method rely on frequency domain measurements of the scattering network parameters performed with a vector network analyzer (VNA). The pulse time domain characteristic is synthesized, using MATLAB software, through the inverse Fast Fourier Transform of the scattering parameters from the VNA. The breast phantoms in our experiment are built of liquid and solid materials as in Table 1. The vector network analyzer as we said serves as transmitter and receiver. The personal computer (PC) is used for signal processing and also controls the VNA and antenna positions.

Experiment setup. To investigate tumor detection and localization, as well as the influence of the antenna, the experimental arrangements are shown in Figure 4-1. The first experiment is designed for initial verification of tumor detection and localization in a 2-D plane and incorporates a monopole antenna. To study the feasibility of using a more efficient antenna, the test setup in Fig. 2 is developed. In all experiments, an 8720C vector network analyzer (Agilent Technol., Palo Alto, CA) is connected to the antenna with a 50 Ω - coaxial cable. The setup is surrounded with electromagnetic absorbing material to reduce ambient reflections. The antennas illuminate the phantom, and S11 is recorded as the frequency is

varied from 50 MHz to 20 GHz (monopole) or from 1 to 18 GHz (horn). Data are recorded at 401 frequency points, and 128 measurements are averaged at each frequency. The phantom is rotated in 16 increments of 22.5° to simulate scanning the antenna around the pipe, and reflections are observed after each rotation. Measuring their performance [9], The antenna is placed 10 cm from the phantom, as finite-difference time-domain (FDTD) simulations [10] indicate that time signatures of the radiated fields do not change with increased distance from the antenna (i.e., the phantom is illuminated with fields having the same time signatures). A horn antenna is used in the second experimental arrangement, specifically an EMCO model 3115 double-ridged waveguide antenna (EMC Test Syst., Austin, TX), which is a linearly polarized broad-band antenna designed to operate from 1 to 18 GHz. The gain at a distance of 1 m from the horn varies from 5.6 dBi at 1 GHz to 16.5 dBi at 16 GHz [11]. The E and H plane beam widths are approximately 60° at 1 GHz, decreasing to 40° at 5 GHz [11]. An appropriate separation between the antenna and phantom is determined by examining reflections from a metal plate placed between 120 and 150 cm from the end of the horn. At distances of 140 cm and greater, the time signatures of the reflections from the plate do not change significantly. The antenna-object separation is larger than expected for the imaging application; a more practical distance will result from both use of an immersion liquid and design of an application-specific antenna.

RESULTS AND DISCUSSION:

Process Flow Diagram of con-focal Algorithm.

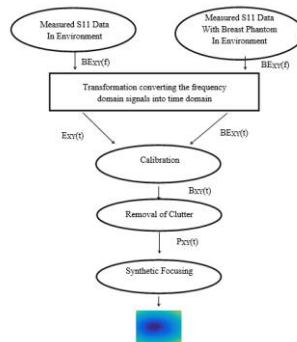


Figure 1. Process Flow Diagram of Algorithm

As discuss in below, to create the image of tumor confocal algorithm is used. Two sets of frequency domain data are obtained from the VNA at antenna position(s);

i. In the **Environment** $E_{XY}(f)$ (involves reflections from different sources which are used for experimental work, i.e. VNA, PC, X-Y Positioner, surroundings etc.)

ii. In the presence of **Breast phantom** $BE_{XY}(f)$ (different materials simulated as tumor in environment)

The frequency domain measurements (i) and (ii) at antenna positions are transformed into time domain by Inverse Fast Fourier Transform (IFFT). The obtained time domain signals $E_{XY}(f)$ & $BE_{XY}(f)$ are then calibrated in the calibration process which involves subtracting the response of the Environment $E_{XY}(f)$ with that of the Breast phantom in environment $BE_{XY}(f)$ to remove the Environment signal(s) $E_{XY}(f)$ so that we can get approximate Breast Phantom signal(s) $BE_{XY}(f)$.

The Breast Phantom signal(s) $B_{XY}(f)$ still contains reflection due to the antenna. To delete, or reduce the reflections due to antenna, the Breast Phantom signal(s) $B_{XY}(f)$ are averaged and the averaged signal is then subtracted to each of the Breast Phantom signal(s) $B_{XY}(f)$. The signal(s) obtained after subtraction are called the Processed signal(s) $P_{XY}(f)$. The Processed signal(s) $P_{XY}(f)$ are synthetically focused to generate the approximate image of Breast Phantom containing tumor.

To evaluate the effectiveness of Confocal Microwave Imaging, the algorithm is written in MATLAB to generate the results of different materials used in our experiment as tumor. After the backscatter signals were transformed into time domain, confocal algorithm is applied, where first calibration of the signals has been carried and the environment response is removed to get the approximate Breast Phantom Response.

After getting the approximate Breast Phantom response, synthetic focusing is performed to generate the image of Breast phantom containing tumor. The results obtained by the experiment performed which are evaluated using MATLAB. The analysis of the result is discussed to assess the effectiveness of the confocal microwave imaging algorithm. The Image of the intensity

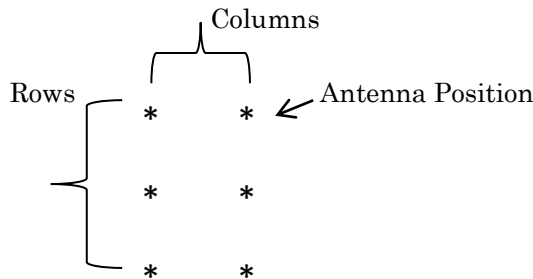
values when the antenna is subjected to the Breast Phantom (environment containing wood as tumor), where Wood is taken as tumor at a depth of 1cm and 3 cm respectively.

Explanation of the Process Flow

Frequency domain data (scattering parameters) is obtained from VNA when antenna is exposed to the environment and when antenna is exposed to the breast phantom in environment. The frequency domain data $E_{XY}(f)$ & $BE_{XY}(f)$ are then transformed to time domain for further processing. The details of each process are discussed below;

i. Transformation:

The antenna is excited with a sweep signal generated by the Vector Network Analyzer (VNA), at 6 different positions in a grid (2 x 3) of covered area 100 mm by 100 mm as shown in Figure 4-3, at different height (1cm and 3cm) from tumor.



The frequency domain data (Environment $E_{XY}(f)$ and Breast Phantom in Environment $BE_{XY}(f)$) obtained from the VNA is first windowed using the Hamming window. A Hamming window is applied to the signal(s) to reduce the level of side lobes. The obtained signal is then transformed into time domain by taking the Inverse Fast Fourier Transform (IFFT) of the signal(s).

$$E_{XY}(f)_{windowed} = E_{XY}(f) * W$$

$$BE_{XY}(f)_{windowed} = BE_{XY}(f) * W$$

$$E_{XY}(t) = \text{iffit} (E_{XY}(f)_{windowed})$$

$$BE_{XY}(t) = \text{iffit} (BE_{XY}(f)_{windowed})$$

Where;

W is the Hamming window signal; XY are the antenna positions defined by row X and column Y in a grid. The grid is represented as a matrix of 3 rows and 2 columns. For 6 antenna positions, the matrix is as follows;

$$\begin{bmatrix} (1,1) & (1,2) \\ (2,1) & (2,2) \\ (3,1) & (3,2) \end{bmatrix}$$

$E_{xy}(t)$ and $BE_{xy}(t)$ are the time domain signals for Environment and Breast phantom in environment at time t respectively. Therefore for 6 antenna positions $E_{xy}(t)$ and $BE_{xy}(t)$ can be represented as;

$$\begin{bmatrix} E_{11}(t) & E_{12}(t) \\ E_{21}(t) & E_{22}(t) \\ E_{31}(t) & E_{32}(t) \end{bmatrix} \quad \begin{bmatrix} BE_{11}(t) & BE_{12}(t) \\ BE_{21}(t) & BE_{22}(t) \\ BE_{31}(t) & BE_{32}(t) \end{bmatrix}$$

ii. Calibration:

The calibration process involves subtracting the response of the Environment with that of the Breast phantom in environment to remove the Environment signal(s) so that we can get approximate Breast Phantom signal(s) This subtraction generates a higher peak at the location of the tumor by reducing the environment response from the target signal. The subtracted signal contains the Breast phantom signal [18-19].

$$B_{XY}(t) = BE_{XY}(t) - E_{XY}(t)$$

Where $B_{XY}(t)$ is the Breast phantom signal at time t for 6 antenna positions.

$$\begin{bmatrix} B_{11}(t) & B_{12}(t) \\ B_{21}(t) & B_{22}(t) \\ B_{31}(t) & B_{32}(t) \end{bmatrix}$$

iii. Clutter Removal:

The Breast phantom signals $B_{XY}(t)$ at location X and Y, still contains reflections dominated due to the antenna and the environment. In order to reduce the reflections due to antenna and environment, the Breast Phantom signal(s) $B_{XY}(t)$ are first averaged. The averaging is done by adding the Breast Phantom signal(s) $B_{XY}(t)$ in a given row of grid (6 x 6), and dividing it with the total number of antenna positions in that row N (total of 6 antenna positions in a given row for our experiment). These signals are known as the averaged signals $A_x(t)$ [18];

$$A_x(t) = \frac{\sum_{Y=1}^N B_{XY}(t)}{N}$$

Where, N is the total number of antenna position in a row.

$A_x(t)$ is the average signal at row X at time t. for 3 rows the signals $A_x(t)$ can be represented as;

$$\begin{bmatrix} A_1(t) \\ A_2(t) \\ A_3(t) \end{bmatrix}$$

The averaged signals $A_1(t)$ are then subtracted to each of the Breast Phantom signal(s) $B_{XY}(t)$. The subtracted signals are known as the Processed Signal(s) $P_{XY}(t)$.

$$P_{XY}(t) = B_{XY}(t) - A_1(t).$$

$P_{XY}(t)$ is the processed signal(s) at location XY at time t. For 6 antenna positions the signals $P_{XY}(t)$ can be represented as;

$$\begin{bmatrix} P_{11}(t) & P_{12}(t) \\ P_{21}(t) & P_{22}(t) \\ P_{31}(t) & P_{32}(t) \end{bmatrix}$$

The processed signals(s) $P_{XY}(t)$ will then be used to generate the intensity values at time t for the formation of image. For generating the intensity values, apart from the processed signals we also need the round trip time. For getting the round trip time we need to perform synthetic focusing which is discussed in detail.

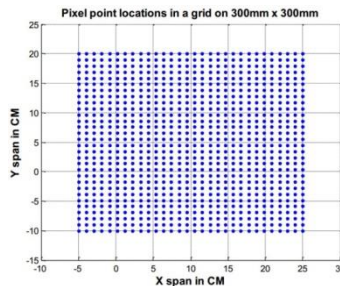
iv. Synthetic Focusing:

The synthetic focusing is performed by computing the round trip time. In order to evaluate the round trip time following steps were performed;

- a) Generate pixel points.
- b) Evaluate the distance from each antenna position to each pixel point
- c) Generate the round trip time.

a) Generate Pixel points

To generate the pixel points $F(x_i, y_j)$ at coordinates x_i and y_j , we considered an area of (300 mm by 300 mm) rather considering the area covered by the antenna positions (100mm by 100mm) for better resolution of the image. Figure 4-4 shows the pixel points (represented by blue dots) locations in a covered area of 300mm by 300mm.



b) Evaluate the distance from each antenna position to each pixel point

The distance(s) $D_{XY}(x_i, y_j)$ of each antenna position XY to the pixel (x_i, y_i) were evaluated using the following equation [18];

$$D_{XY}(x_i, y_j) = 2\sqrt{(X - x_i)^2 + (Y - y_i)^2 + h^2}$$

Where;

h is the height of the antenna (1cm or 3cm) from the tumor;

x_i and y_j define the coordinates of the pixel points;

The antenna positions are defined by X and Y;

$D_{XY}(x_i, y_j)$ is the round trip distance for antenna position XY to the pixel.

In the experiment we have used single antenna as transmitter and receiver. Therefore the distance covered by the transmitter to each pixel point and by the receiver to each pixel point will be same. Therefore we multiply the distance by 2. Figure 2,3 shows the method for finding the round trip distance from each antenna position to each pixel point.

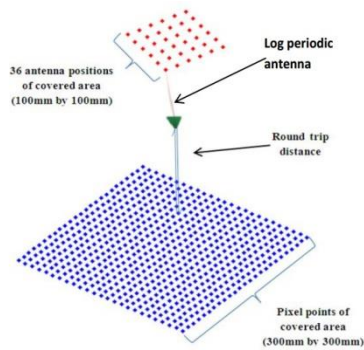


Figure 2. Representation of finding the round trip distance of each Antenna position to the Pixel points

c) Generate the round trip time.

The round trip time is finally calculated for antenna position XY at pixel (xi , yj) by the following equation;

$$t_{xy}(xi,yj) = \frac{D_{xy}(xi ,yj)}{c/\sqrt{\epsilon_r}}$$

Where c is the speed of light in cm/s;

ϵ_r is the permittivity of the medium (air $\epsilon_r = 1$ for our experiment)

$t_{xy}(xi , yj)$ is the round trip time from antenna position XY to pixel (xi , yj)

v. Image Formation

As discussed before to generate the intensity values to form the image, apart from the processed signal $P_{xy}(t)$, time values are also needed. After calculating the time values $t_{xy}(xi , yj)$ for each antenna position XY at pixel (xi , yj), the Intensity values are generated for each pixel points by evaluating the signal value of the processed signal $P_{xy}(t)$ at time $t_{xy}(xi , yj)$. Mathematically the intensity values at pixel (xi , yj) is represented as

$$I(xi , yj) = \left[\sum_{X=1}^r \sum_{Y=1}^c P_{XY}(t_{XY}(xi , yj)) \right]^4$$

Where;

r is the total number of antenna positions in a row;

c is the total number of antenna positions in a column;

$I(x_i, y_j)$ is the intensity value at pixel point (x_i, y_j) .

The reason behind taking the 4th power instead that the second power as in [13] has been done after several tests by research group at the University of Calgary [39] since they observed that the 4th power proved to suppress the clutter but affected the size of tumor whereas in [13] the 2nd power did not suppress the clutter as compared to the 4th power and the size of the tumor was also not affected.

6. Image Reconstruction: To form the image, the processed signals are synthetically focused at a specific point in the breast. First, distances from each antenna to the focal point are computed and converted into time delays. The time delays are used the focal point locations extend from the lower boundary of the skin into the breast interior. With the cylindrical system, estimates of the skin location bound the focal points [42].

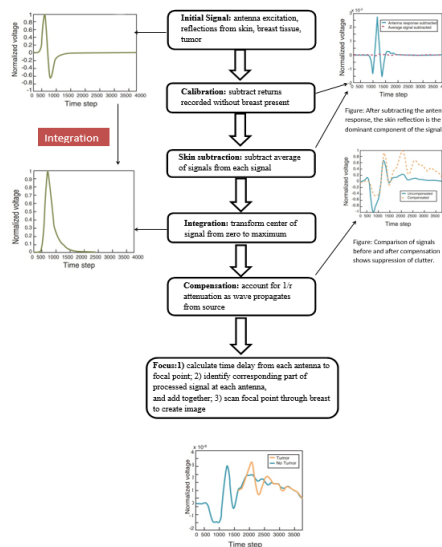


Figure 3. Processed signals with and without tumor present in breast model.

This method avoids nonlinear inverse scattering techniques that may be complex and computer intensive. However, it does not provide profiles of the permittivity, but only identifies regions of increased scattering due to a small region of different permittivity. To acquire the data, the breast is illuminated with an ultra-wideband pulse, and the same antenna collects the backscattered waves. This process is repeated for multiple antenna positions. A time-shift-and-add algorithm is applied to the set of pulses recorded at the antenna output in all positions. The time delay for the round trip to a given point in the test domain is computed for each antenna position. Next, the signals with the appropriate time delays are summed up. The focal point is scanned to a new location and the focusing process is repeated. This procedure ensures that signals from a given pixel or voxel in the test domain add coherently. Signals from scatterers in other locations add incoherently, which tends to reduce clutter. Thus, a small scatterer can be picked up, if it has sufficiently large contrast compared to a random heterogeneity within the test domain. The same principle is used in several synthetic aperture ground penetrating radar systems. One of the significant advantages of this approach is that high resolution can be obtained provided that a sufficiently wideband pulse can be used. In the system introduced by Hagness and colleagues, the woman to be scanned lies on her back and antennas are placed on the flattened breast surface. A comprehensive numerical evaluation of performance of this system has been performed with the finite difference time domain (FDTD) method. Initial work has suggested the feasibility of detecting tumors as small as 2 mm at depths of up to 5 cm. resistively loaded bowtie antennas were developed for added sensitivity to small tumors. Observation of the cross polarization was proposed for detection of tumors in the presence of strongly scattering planar objects such as the chest wall. The use of ultra-wideband signals provides ultra-wideband reflections, or microwave signatures. It was suggested that if various tumor shapes are associated with specific microwave signatures, then this characteristic may be used to aid in diagnosis or detection. Further investigations for more realistic MRI-based 2D models were carried out. The successful detection of small tumors in this more complex environment was demonstrated. Initial experimental feasibility testing is ongoing. An alternative cylindrical

system based on the same principle has also been developed. Extensive numerical modeling and experimental feasibility assessments indicate that this system is also very promising. Since the theoretical results in terms of detection of small tumors appear to be comparable for the planar and our system, the more detailed description that follows is limited to our system.

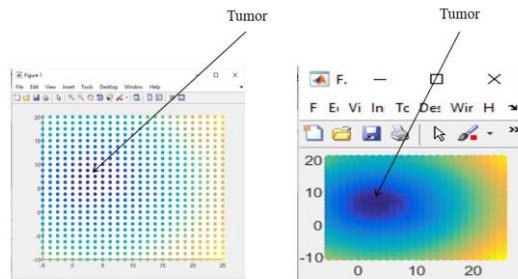


Figure 4. Low resolution **Image 5.** High resolution Image

Figure 4,5 shows the responses for the materials as tumor for antenna distances at 1cm and 3cm. It is noted that the effectiveness of the confocal algorithm signifies the tumor responses for all the materials in Table 1 chapter 4, but the antenna distance from the object indicated that certain materials (PVC, glass, plastic, rubber, wood) tend to generate more scatter in the surrounding. The significance of the amount of scatter is dependent on the size and the electrical conductivity of the material. Since the materials (PVC, glass, plastic, rubber and wood) are less electrically conductive as compared to water copper, the transmitted signals from the antenna dissipate in the surrounding. As the size of the material increase, larger area is covered and more signals is dissipated in the environment. If the amount of additional scatter is more, then the size of the tumor detected is affected which generates problems in identifying the actual size of tumor.

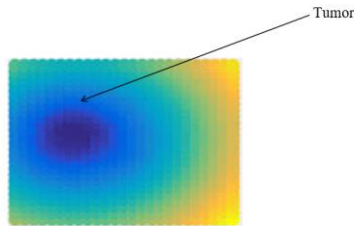


Figure 6. Output Image of Confocal Microwave Imaging Algorithm.

Performance Measures. To examine the influence of each step in the signal processing sequence, the backscatter recorded at a single antenna is studied in detail. To follow the enhancement of the tumor response during the image formation process, we compare the peak-to-peak tumor response with that of the total signal at each of the four steps. Estimation of the peak-to-peak tumor response requires additional simulations. The tumor is removed from the breast model, and backscatter is recorded at each antenna in the selected row. We isolate the tumor response by subtracting the tumor-free returns recorded at each antenna location from the recorded signals for the model containing a tumor. The average tumor response for the selected row of antennas is computed, and used to calibrate the tumor responses recorded at each antenna in the row. The peak-to-peak of the tumor response is calculated initially and after each signal processing step. These results are compared with those calculated for the total signal. To investigate tumor detection, images are formed for the tumor-bearing breast model and the tumor-free model. Comparison of results ensures that tumors are detected only when present in the models. The influence of the number of antennas is examined by comparing images reconstructed with the full set of antenna positions and the limited set (6 antenna positions). The results of changing array span and tumor location are also examined. Several measures related to the tumor response and clutter are defined to evaluate the images. To investigate tumor localization, the location and FWHM extent of the tumor response are determined. Two signal-to-clutter (SC) ratios are defined to quantify the magnitude of the tumor response. The within-breast SC ratio compares the maximum tumor response with the maximum clutter response in the same image. The maximum clutter is determined by

locating the maximum pixel value outside of the volume containing the imaged tumor (defined by twice the extent of the FWHM response of the tumor). The between-breast SC ratio compares the maximum tumor response with the pixel intensity at the same location in the image formed without a tumor present. To provide additional insight into the clutter behavior, the mean and standard deviation of the clutter are computed.

CONCLUSION:

Microwave imaging techniques offer the potential of low cost, non-invasive screening tool and within a non-harmful spectrum range. In this report, experimental results of UWB microwave imaging system for Radar based breast cancer detection is presented, whereby we confirm the detection of tumor with 10 - 20 mm diameter and producing the viability of using the confocal algorithm for early breast cancer detection. We analyze the Confocal Microwave Imaging Algorithm for different permittivity of materials to investigate its effectiveness. The results show that the materials i.e. Water, silicon, PVC, copper, rubber, wood, glass and plastic used in the experiment tend to generate more scatter in the surrounding due to difference in electrical conductivity between each of them. The results also show that the level of intensity changes when the distance of the antenna is changed from 1cm to 3cm from the materials (tumor), because of the low power level recorded as the signal is received. The results also signify the effect of the electrical permittivity in contrast between the normal and cancerous tissue. Due to the increase in the ratio of the dielectric contrast, different materials give more scatter, with water having a higher dielectric ratio with air giving a higher amount of scatter and PVC with a lower dielectric ratio with air recording a lower amount of scatter at the antenna. If the amount of additional scatter is more, then the size of the tumor located will be affected which will generate problems in identifying the actual size of tumor. The results signify that the distance of the antenna from the tumor and the permittivity of the medium directly affects the location and the size of the tumor when Confocal Microwave Imaging algorithm is considered. Although the algorithm used for our experimental work is computationally simple but it has limitations,

such as it provides limited performance in terms of image resolution and clutter rejection.

REFERENCES:

- [1] Elise C. Fear, Susan C. Hagness and Maria A. Stuchly, "Confocal Microwave Imaging for Breast Cancer Detection: Localization of Tumors in Three Dimensions." Vol. 49, no. 8, Aug 2002
- [2] Novant Medical Group [online] (2011) Available from: <http://www.novantmedicalgroup.org> [accessed 15th June 2011].
- [3] Novant Medical Group [online] (2011) Available from: <http://www.novantmedicalgroup.org> [accessed 15th June 2011].
- [4] Breast cancer image. Available from: <https://www.gettyimage.com> [accessed 20th may 2019].
- [5] T. S. England and N. A. Sharples, "Dielectric properties of the human body in the microwave region of the spectrum," *Nature*, vol. 163, pp. 487-488, 1949.
- [6] T. S. England, "Dielectric properties of the human body for wavelength in the 1-10 cm range," *Nature*, vol. 1466, pp. 480-481, 1950.
- [7] A. J. Surowiec, et al., "dielectric-properties of breast-carcinoma and the surrounding tissues," *Ieee Transactions on Biomedical Engineering*, vol. 35, pp. 257-263, 1988
- [8] M. Brown, F. Houn, E. Sickles, and L. Kessler, "Screening mammography in community practice," *Amer. J. Roentgen.*, vol. 165, pp. 1373-1377, Dec. 1995.
- [9] P. T. Huynh, A. M. Jarolimek, and S. Daye, "The false-negative mammogram," *Radiograph.*, vol. 18, no. 5, pp. 1137-1154, 1998.
- [10] J. G. Elmore, M. B. Barton, V. M. Mocerri, S. Polk, P. J. Arena, and S. W. Fletcher, "Ten-year risk of false positive screening mammograms and clinical breast examinations," *New Eng. J. Med.*, vol. 338, no. 16, pp. 1089-1096, 1998.
- [11] M. Sabel and H. Aichinger, "Recent developments in breast imaging," *Phys. Med. Biol.*, vol. 41, pp. 315-368, March 1996.
- [12] S. H. Heywang-Kobrunner, "Nonmammographic breast imaging techniques," *Curr. Opinion Radiol.*, vol. 4, pp. 146-154, Oct. 1992.
- [13] A. J. Surowiec, S. S. Stuchly, J. R. Barr, and A. Swarup, "Dielectric properties of breast carcinoma and the surrounding tissues," *IEEE Trans. Biomed. Eng.*, vol. BME-35, pp. 257-263, Apr. 1988.
- [14] W. T. Joines, Y. Zhang, C. Li, and R. L. Jirtle, "The measured electrical properties of normal and malignant human tissues from 50 to 900 MHz," *Med. Phys.*, vol. 21, pp. 547-550, April 1994.
- [15] S. S. Chaudhary, R. K. Mishra, A. Swarup, and J. M. Thomas, "Dielectric properties of normal and malignant human breast tissues at radiowave and microwave frequencies," *Indian J. Biochem. Biophys.*, vol. 21, pp. 76-79, February 1984.
- [16] S. C. Hagness, K. M. Leininger, J. H. Booske, and M. Okoniewski, "Dielectric characterization of human breast tissue at microwave frequencies," presented at the 2nd World Congr. Microwave and Radio Frequency Processing, Orlando, FL, Apr. 2000.
- [17] Available from: www.verywellhealth.com [accessed 29th may 2019].

Samiran Kumar Mandal, Szal Kumar Samadder– **A Comprehensive Study on Microwave Imaging System for Breast Cancer Detection and Confocal Microwave Imaging**

- [18] Abdul-Satter, Zubaida “Experimental analysis on effectiveness of confocal algorithm for radar based breast cancer detection. Durham thesis, durham university, Available at Durham E-thesis online: <https://etheses.dur.ac.uk/3531/>
- [19] D.J. Watmough and K.M. Quan, “X-ray mammography and breast compression”, *Lancet*, 340, p.122, 1992.
- [20] D. D. Stark and W. G. Bradley, Jr., *Magnetic Resonance Imaging*, 2nd ed., Mosby-Year Books, St. Louis, 1992.
- [21] M. A. Brown and R. C. Semelka, *MRI: Basic Principles and Applications*, 2nd ed., Wiley-Liss, New York, 1999.
- [22] S. C. Bushong, *Diagnostic Ultrasound*, McGraw-Hill, New York, 1999.
- [23] D. Paquette, J. Snider, F. Bouchard, I. Olivotto, H. Bryant, K. Decker, and G. Doyle, “Performance of screening mammography in organized programs in Canada in 1996,” *Can. Med. Assoc. J.*, vol. 163, pp. 1133-1138, 2000.
- [24] M. L. Finkel, *Understanding the Mammography Controversy: Science, Politics, and Breast Cancer Screening*, 1st edition, Greenwood Publishing Group, Inc., 2005.
- [25] Breast Health Online [online] (2011) Available from: <http://www.imaginis.com/breasthealth>[accessed 20th June 2011]
- [26] Emorial Hospital of Texas County [online] (2011) Available from: <http://www.mhtcguymon.org/> [accessed 20th June 2011].
- [27] S.C. Hagness, A. Taflove, and J.E. Bridges, “Three-dimensional FDTD analysis of pulsed microwave confocal system for breast cancer detection: design of an antenna-array element”, *IEEE Trans. Antennas Propagat.*, vol. 47, pp. 783-791, May 1999.
- [28] E.C. Fear and M.A. Stuchly “Microwave detection of breast cancer,” *IEEE Trans Microwave Theory Tech.*, vol. 48, pp. 1854-1863, Nov. 2000.
- [29] E.C. Fear and M.A. Stuchly, “Microwave system for breast tumor detection,” *IEEE Microwave Guided Wave Lett.*, vol. 9, pp. 470-472, Nov. 1999.
- [30] Xu Li, Student Member, IEEE, and Susan C. Hagness, Member, IEEE “A Confocal Microwave Imaging Algorithm for Breast Cancer Detection” *IEEE microwave and wireless components letters*, vol. 11, NO. 3, MARCH 2001
- [31] Vitaliy Zhurbenko, “Challenges in the Design of Microwave Imaging Systems for Breast Cancer Detection”, *Advances in Electrical and Computer Engineering*, Volume 11, Number1, 2011.
- [32] P. Meaney, M. Fanning, D. Li, S. Poplack, and K. Paulsen, “A clinical prototype for active microwave imaging of the breast,” *IEEE Transactions on Microwave Theory and Techniques*, vol. 48, no. 111, pp.1841–1853, 2000.
- [33] P. Meaney, K. Paulsen, J. Chang, and M. Fanning, “Initial microwave imaging experiments in ex-vivo breast tissue,” *Proceedings of the First Joint BMES/EMBS Conference*, 1999, vol. 2, p. 1130, 1999.
- [34] D. Li, P. Meaney, T. Reynolds, S. Pendergrass, M. Fanning, and K. Paulsen, “A broadband microwave breast imaging system,” *Proceedings of the IEEE 29th Annual Bioengineering Conference*, 2003, pp. 83–84, 2003.
- [35] Sara M. Salvador, Giuseppe Vecchi, “Experimental Tests of Microwave Breast Cancer Detection on Phantoms”, *IEEE* 2009
- [36] S.M. Salvador, G. Vecchi, G.Pagana, C.Cacciatore, R.Maggiara, E.Attardo, "A comparison between two algorithms for microwave breast cancer detection", *LACE/DELEN*, Politecnico di Torino, C.so Duca degli Abruzzi 24, 10129 Torino, Italy.

- [37] A. Lazaro, D. Girbau, and R. Villarino” simulated and experimental investigation of microwave imaging using uwb” Progress In Electromagnetics Research, PIER 94, 263{280, 2009
- [38] D. W. Winters, J. D. Shea, E. L. Madsen, G. R. Frank, B. D. Van Veen, S. C. Hagness, “Estimating the Breast Surface using UWB Microwave Monostatic Backscatter Measurements” IEEE Trans. Biomed. Eng., vol. 55, no. 1, pp. 247 –256, Jan.
- [39] D. W. Winters, B. D. Van Veen, and S.C. Hagness, “UWB Microwave Imaging for Breast Cancer Detection: An Algorithm for Estimating the Breast Surface”, IEEE Ant. Prop. Symp., pp. 267 - 270, July 2006.
- [40] Dielectric of various materials [online Available from: <http://www.thelenchannel.com/1dielectric.php> [accessed 20th June 2011].
- [41] X. Li, E. J. Bond, B. D. Van Veen, and S. C. Hagness, “An overview of ultrawideband microwave imaging via space-time beamforming for early-stage breastcancer detection,” IEEE Ant. Prop. Mag., Vol. 47, pp. 19-34, Feb. 2005.
- [42] “Microwave detection of breast tumors: Comparison of skin subtraction algorithms,”Proc. SPIE, vol. 4129, pp. 207–217, 2000.